Available online at www.sciencedirect.com
ScienceDirect
Polymer 48 (2007) 6041–6048
polymer
www.elsevier.com/locate/polymer

In situ AFM investigation of crazing in polybutene spherulites under tensile drawing

C. Thomas, V. Ferreiro[1], G. Coulon, R. Seguela*

Laboratoire Structure et Propriétés de l'Etat Solide, CNRS, Université de Lille1, Batiment C6, 59655 Villeneuve d'Ascq, France

Received 16 May 2007; received in revised form 11 July 2007; accepted 20 July 2007
Available online 1 August 2007

Abstract

This report deals with the study of the plastic deformation processes of semi-crystalline polymers at the micrometric and nanometric scales by atomic force microscopy. Capturing images from the same locus of the sample as a function of strain allows *in situ* observation of the processes. New experimental findings regarding initiation, growth and coalescence of crazes in poly(1-butene) are reported. The benefits of the technique are emphasized in comparison with previous studies carried out by transmission electron microscopy on ultra-thin films of various semi-crystalline polymers. The present situation is claimed to be closely representative of bulk deformation owing to the much greater sample thickness in comparison with the characteristic craze size. The occurrence of crazes oblique to the principal tensile stress is discussed in terms of triaxiality of the local stress field within the spherulites.

Keywords: Poly(1-butene); Atomic force microscopy; Crazing

1. Introduction

Crazing is one of the two major processes of plastic deformation of solid polymers in competition with shear banding. Crazing is a cavitational process which only occurs under tensile loading, owing to the negative hydrostatic stress component, and which can be described as a three-stage process [1,2]. This is valid for both glassy and semi-crystalline thermoplastic polymers. Initiation proceeds by cavity nucleation between chains which separate from each other without chain scission. The craze gradually opens by extension of the chain coils and pulling them from the bulk material giving rise to microfibrils bridging the free surfaces of the initial unstable cavity. The large contrast between weak inter-chain and strong intra-chain interactions is the basic reason for the occurrence of this phenomenon typical to polymers. Then the craze propagates normal to the main stress direction by transmission of the anelastic deformation to the bulk material ahead of the craze tip. As the craze grows by generation of new microfibrils at the craze tip, the microfibrils within the craze core are gradually drawn up to their ultimate draw ratio. Microfibril rupture finally turns the craze into a crack by either chain scission or chain disentanglement, depending on chain length and temperature.

Glassy homopolymers are chemically and physically homogeneous down to the molecular scale, so that crazing should necessarily initiate at the scale of molecular density fluctuations, or may benefit from processing defects such as porosity, local chain orientation or surface defects.

Semi-crystalline polymers are intrinsically heterogeneous materials at a nanometric scale in which crazing can easily be initiated in the more compliant amorphous phase or at the crystal/amorphous interface, particularly for temperatures above the glass transition when the amorphous phase is rubbery. Notwithstanding, the crazing propensity of semi-crystalline polymers depends on their chemical nature, macromolecular architecture and crystalline structure. Polymers with

* Corresponding author.
E-mail address: roland.seguela@univ-lille1.fr (R. Seguela).
[1] Present address: Research & Development Center, ARKEMA FRANCE, 27470 Serquigny, France.

0032-3861/$ - see front matter © 2007 Elsevier Ltd. All rights reserved.
doi:10.1016/j.polymer.2007.07.062

strong inter-chain bonds such as polyamides are less craze-prone than polyolefins which only have van der Waals inter-chain interactions [3]. This is why nylons are often filled with either soft or hard particles which promote the nucleation of profuse crazes and shear bands owing to the stress concentration generated at the particle/matrix interface [4–7]. High chain entanglement density and/or high molar weight are favorable factors for craze-resistance due to generation of a high degree of molecular connection between neighbor crystalline lamellae [1]. Regarding the crystalline structure, polypropylene is well known to be more craze-prone if the β crystalline phase is promoted during processing at the expense of the thermodynamically stable α phase [8–12]. The physical explanations for this contrasting behavior towards crazing of the two crystalline forms are still hypothetical. The stiffening effect of the cross-hatched lamellar crystals in α spherulites was suspected to be detrimental to craze stability [8,13,14]. In contrast, the lower values of both the elastic limit and the flow stress of the β spherulites as compared with the α ones [15], together with the stronger strain-hardening [16], are beneficial to craze stability which promotes craze multiplication at the expense of crack initiation [17].

It is noteworthy that cavitation and fibrillation in semi-crystalline polymers may also occur without actual crazing [1]. For instance, crossing of shear bands may generate cavitation damage. Besides, Plummer and Kausch [18] showed from Transmission Electron Microscopy that plastic deformation zones involving shear banding and high local drawing can result in fibrillation accompanied with inter-fibril cavitation, such fibrils being roughly one order of magnitude thinner than true craze fibrils. These authors suggested that this process is the one operating in β PP [13]. Similarly, recent *ex situ* investigations by Atomic Force Microscopy of the tensile deformation of nylon 6 showed that plastic flow proceeds via shear bands, before the occurrence of fibrillation at high draw ratios [19,20].

The present work is the first part of a study regarding the plastic deformation behavior of isotactic polybutene, a semi-crystalline polymer closely related to PP, which displays various plastic capabilities depending on the spherulite size [21]. The reported data are concerned with the crazing of polybutene films with large spherulites. A second objective of the work is to benefit from *in situ* AFM observations of the same locus on the investigated sample to follow the various steps of craze development.

2. Experimental

The poly(1-butene) material (PB) from Shell has number- and weight-average molar weights $M_n \approx 28$ kDa and $M_w \approx 174$ kDa. The PB pellets were compression-molded into 100 μm thick sheets at 170 °C for 2 min before cooling at about 20 °C/min. Borrowing from Weynant's isothermal crystallization study [21], sheet pieces were melted again at 170 °C with free-upper surface and subsequently crystallized for 2 h at 80 °C in a temperature-regulated oven. The films were stored for at least 5 days at room temperature prior to investigation in order to promote complete structural transformation of the thermodynamically metastable tetragonal crystals issued from the isothermal crystallization into stable hexagonal crystals [21,22].

The thermal behavior of the material was investigated by Differential Scanning Calorimetry (DSC) using a Diamond Perkin–Elmer apparatus at a scanning rate of 10 °C/min, the sample weight being about 10 mg. The temperature range −20 to 150 °C and the heat flow scale were calibrated from the recording of the melting of high purity indium and zinc samples at the same scanning rate. The peak temperature of the single melting endotherm of the structurally stable films was 123 °C and the weight fraction crystallinity was 0.55, taking a value $\Delta H_f = 120$ J/g [23] for the melting enthalpy of perfectly crystalline isotactic poly(1-butene). The glass transition of the amorphous phase not observable from DSC was characterized by Dynamic Mechanical Thermal Analysis in tensile mode at 1 Hz, using a RSA3 apparatus from TA Instruments. The main relaxation peak occurred at about −20 °C, indicating that the amorphous phase was rubbery at room temperature, *i.e.* the temperature of the *in situ* AFM investigations. The spherulite size was in the range 100–200 μm as measured using the AFM video-camera attachment.

Atomic Force Microscopy observations were performed on a Dimension 3100 apparatus from Digital Instruments operated in Tapping mode™. The Nanoworld silicon SPM sensors (type NCL) had a tip radius less than 10 nm, the nominal spring constant and resonance frequency of the cantilever being, respectively, 48 N m^{-1} and 190 kHz. The height and amplitude images were recorded with a set-point amplitude ratio r_{sp} in the range 0.9–0.95 in order to get topographic contrast [20]. The (512 × 512 pixels) images were obtained by operating the (90 × 90 mm^2) piezoelectric scanner at a scanning rate of 0.5 Hz. The AFM apparatus was equipped with a home-made tensile drawing stage that enabled stepwise deformation of films at constant crosshead speed and holding the sample at chosen constant strains for image recording. The drawing device shown in Fig. 1 consists of a crosshead moving via a stepper motor, the two ends of the sample being clamped on the mobile crosshead and a fixed part of the stage. During straining, the video-camera helps repositioning the AFM head (piezoelectric scanner) above the observation zone of the sample. The dumbbell-shaped samples with gauge length 24 mm and width 5 mm were stretched at room temperature, using a crosshead speed of 1 mm/min. Every time straining was interrupted for the AFM observations, the samples were allowed to relax for a period of 10 min that was long enough for the stress to level off before starting image recording. This equipment is somewhat similar to the manual or motorized ones described by Hild et al. [24], Michler et al. [25], Oderkerk et al. [26] and Bamberg et al. [27], also operated under stepwise stretching–relaxation procedure. The macroscopic strain, ε, was determined from the displacement of the crossheads. The local strain, ε_{local}, at the scale of the spherulites in the direction of the tensile stress was occasionally estimated on optical images from the AFM video-attachment using the displacement of specific items at the inter-spherulitic boundaries.

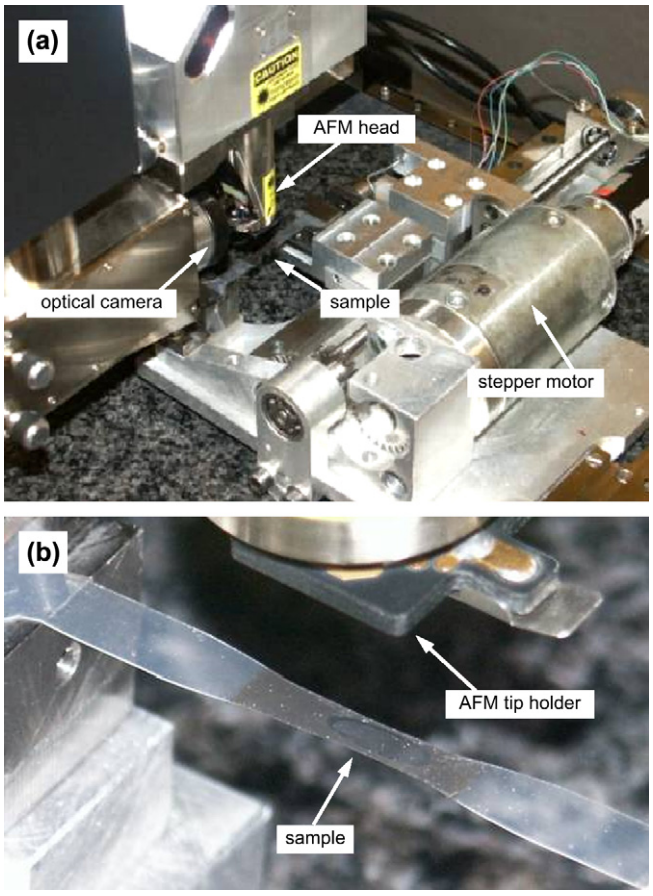

Fig. 1. Motorized stretching stage for *in situ* AFM investigations: (a) overview of the experimental set up; (b) close view of the sample positioning.

All the AFM images have been recorded with the tensile axis vertical.

3. Results

Although the PB films could be one-way stretched in a conventional testing machine up to a macroscopic strain at rupture $\varepsilon_{rupt} \approx 50\%$, stepwise drawing on the AFM stage always ended in early rupture at strain $\varepsilon = 15-20\%$ due to the material relaxation during the long duration of every AFM image recording at constant strain.

Fig. 2 displays optical micrographs from the AFM video-attachment at various strains up to about rupture. The spherulite deformation is roughly uniform at first sight. However, the local longitudinal strain turns out to be significantly different from the macroscopic strain: for instance measurements on the central spherulite of Fig. 2 give $\varepsilon_{local} \approx 10\%$ when $\varepsilon = 6\%$ and $\varepsilon_{local} \approx 25\%$ when $\varepsilon = 15\%$. In parallel, the transverse local strain of the same spherulite is close to naught. Statistical measurements on several spherulites reveal broad distribution of local longitudinal strain about the macroscopic value, and about nil transverse local strain within the experimental accuracy. Besides, *ex situ* measurements of strains through the film thickness indicated that the tensile deformation was not actually compensated by thickness reduction,

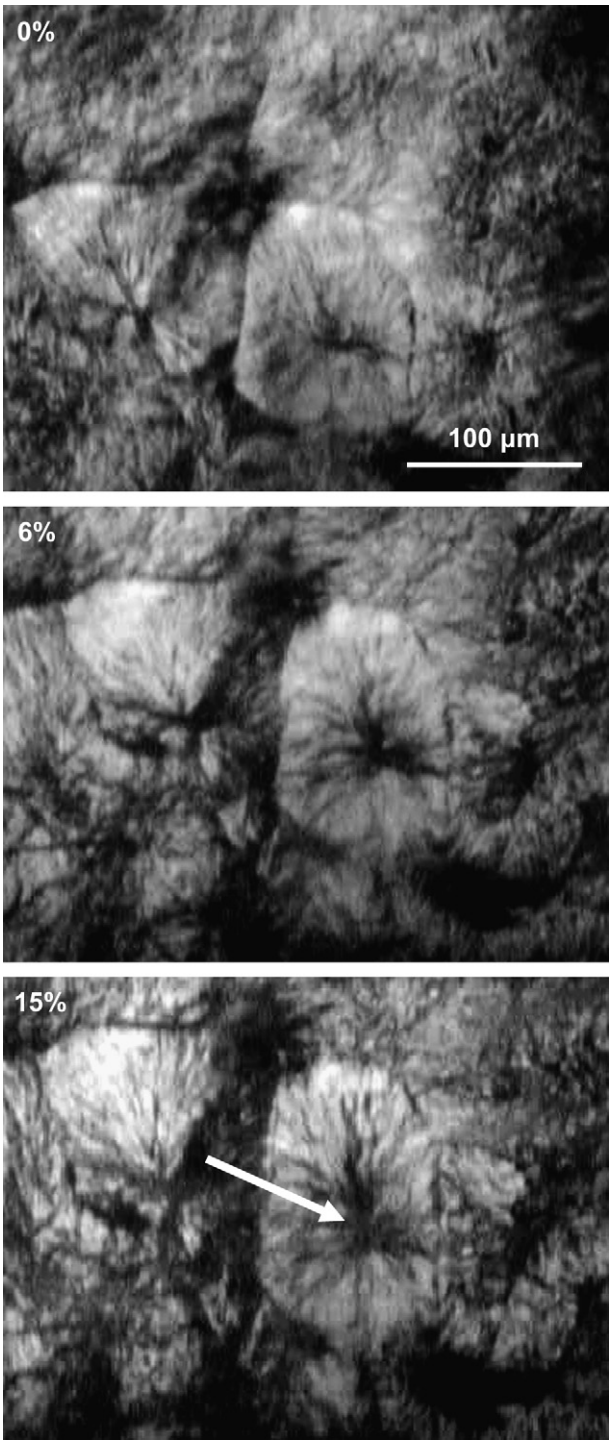

Fig. 2. Optical micrographs from the AFM camera of the PB film surface as a function of macroscopic strain (see the text for details).

within the accuracy of the thickness measurements. These findings first reveal that stretching is accompanied with significant volume strain or cavitation in the spherulites. It is suspected that the well developed radial arrangement of crystalline lamellae builds up a rigid structure which prevents transverse contraction of the spherulites. Second, the large departure between local and macroscopic strains gives evidence of deformation heterogeneities at the scale of the spherulite

size, the cavitation level being different between neighbor spherulites depending on shape and size.

The large scale AFM images in amplitude mode of Fig. 3 give a close up view of the heart of a spherulite enlightening both the structural heterogeneity about the precursory axialite and the radial growth of the crystalline lamellae. Stepwise straining from $\varepsilon = 0\%$ to 15% results in gradual elongation and distortions of the axialite accompanied with ridge formation in the equatorial region of the spherulite, noticeably on the right side of the axialite. The height images of Fig. 4 reveal that the ridged structure arises from the opening of interlamellar lenticular cavities. Also captured in Fig. 4 are the concomitant growth and coalescence of cavities when strain is increased from 10 to 15%, in addition to the opening of new cavities. These cavities are predominantly observed about structural heterogeneities such as defects in the regular stacking of the crystalline lamellae or in the boundary between lamella stacks having different orientations. Both kinds of structural defects are likely to be preferred loci for generating stress concentration.

The predominant development of cavities in the equatorial region of the spherulites with remarkable preservation of the crystalline lamella integrity in the transverse direction, as revealed from Fig. 3, provides rational explanation to the insignificant transverse strain previously mentioned from the analysis of the video-camera recordings (Fig. 2). This observation supports the assumption that the driving force for cavitation lies in the stiffness of the crystalline lamellae which impede transverse contraction of the spherulites.

The close up view of Fig. 5 reveals that the interlamellar cavities are actual crazes with well formed microfibrils bridging the two edges of the cavity. The craze edges consist of intact crystalline lamellae on which the microfibrils are directly anchored. Inside one of the crazes of Fig. 5, a residual lamella

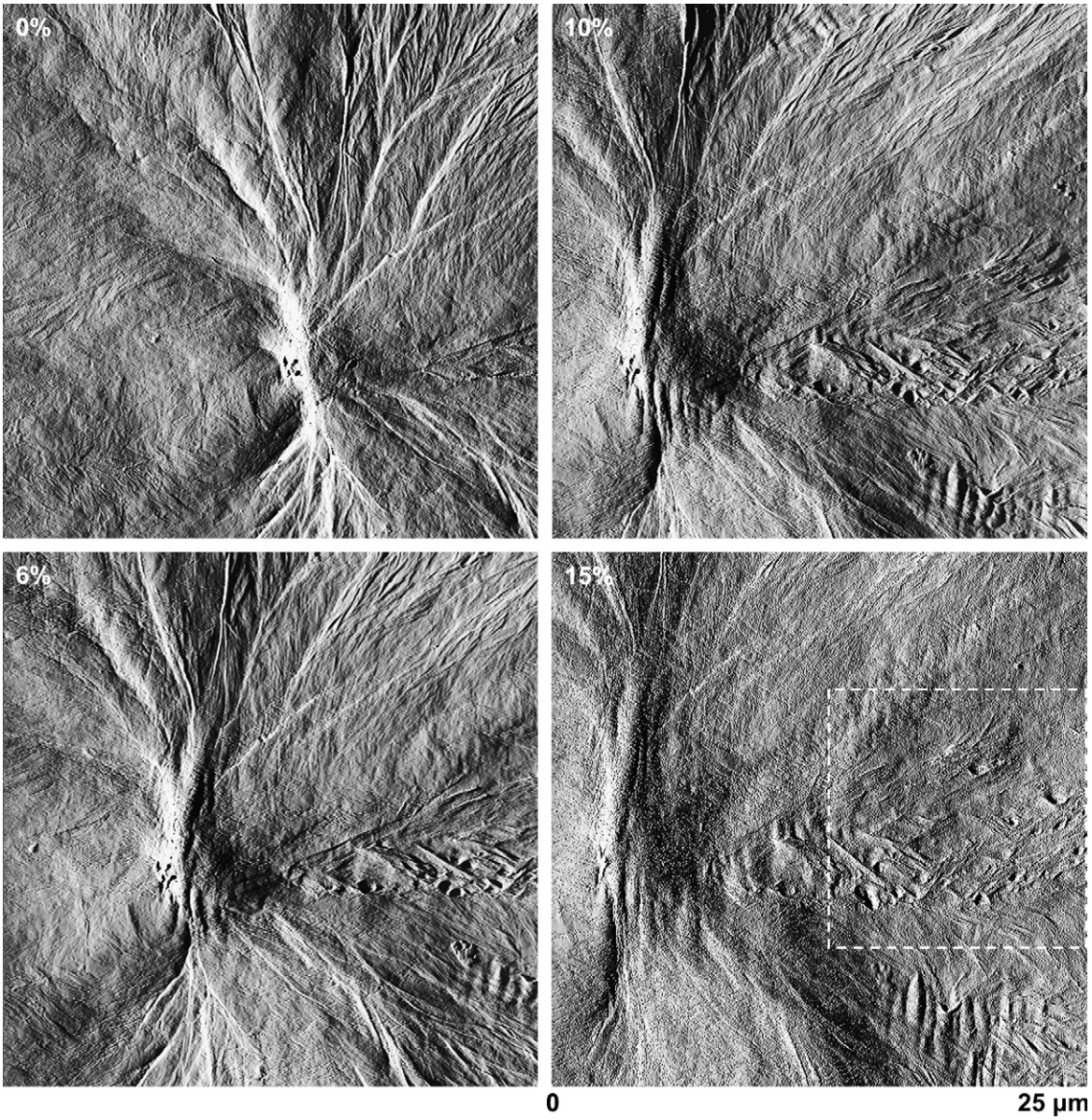

Fig. 3. Large scale AFM amplitude images from the core of a spherulite at strains $\varepsilon = 0\%$, $\varepsilon = 6\%$, $\varepsilon = 10\%$ and $\varepsilon = 15\%$.

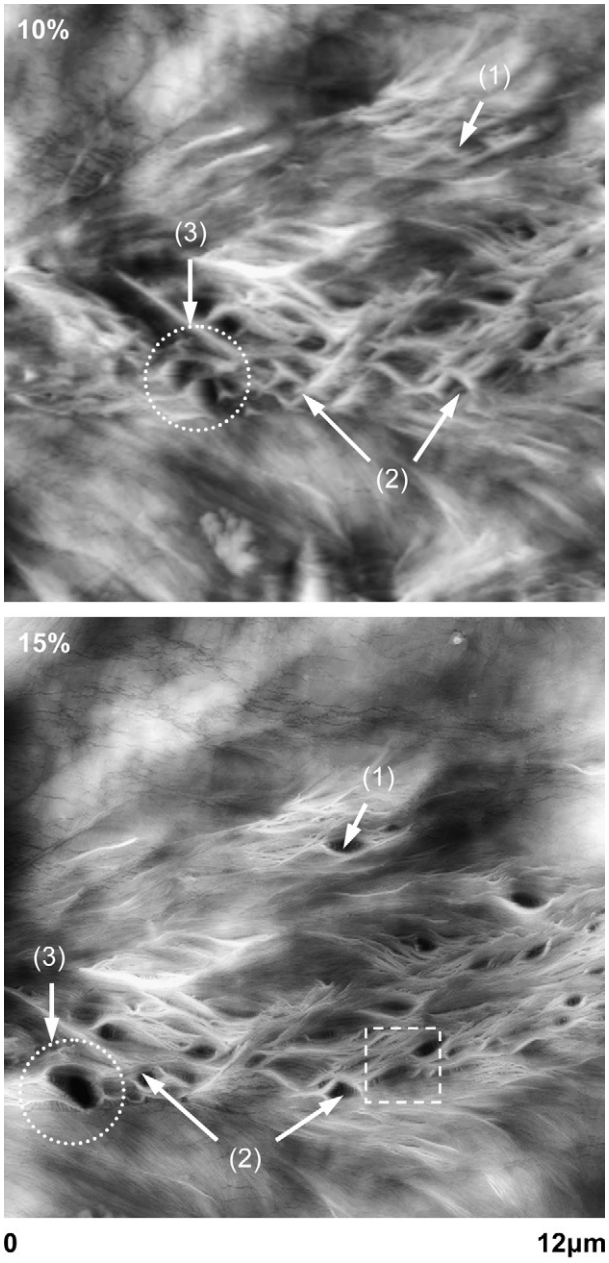

Fig. 4. AFM height images (Z-range = 600 nm) from the selected square area in equatorial region of Fig. 3 for two strain levels $\varepsilon = 10$ and $\varepsilon = 15\%$ (on the images are indicated (1) the opening, (2) the growth and (3) the coalescence of cavities).

appears to be involved in the process of fibrillar transformation, as indicated by the white arrow. The craze structure suggests that crystalline lamellae have undergone chain-unfolding, this process being uniformly stopped at an amorphous–crystal interface on both sides of the craze. However, one cannot assess from this image how many lamellae were involved in the fibrillar transformation process.

It is worth noticing from Fig. 5, and from Fig. 4 as well, that most of the crazes do not open perpendicular to the principal tensile stress, as revealed by the preferred oblique direction with respect to the vertical axis. In parallel, the predominant location of crazes between crystalline lamellae

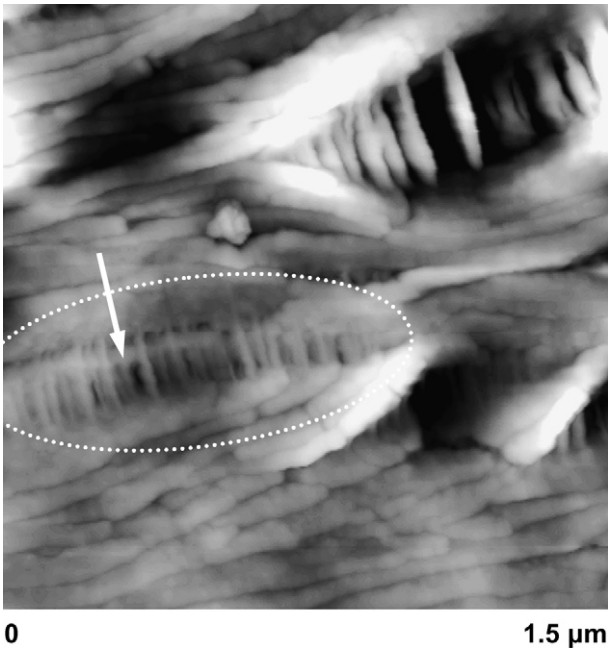

Fig. 5. Small scale AFM height image (Z-range = 500 nm) from the selected square area indicated in Fig. 4 at strain $\varepsilon = 15\%$ (the arrow points at an isolated crystalline lamella involved in the process of fibrillar transformation within a growing craze).

suggests that craze development is strongly influenced by the lamella orientation. Indeed, the stiff crystalline lamellae are likely to generate a triaxial local stress field, where the stress component normal to lamella surface becomes the key factor for craze nucleation in the soft amorphous layer. The present situation strongly contrasts with that of crazes in α and β PP spherulites which mainly grow normal to the principal tensile stress [11,12]. The latter observation includes the polar regions where the crystalline lamellae parallel to the tensile stress are readily crossed by the growing crazes.

Oblique crazes have also been observed in the diagonal regions of the spherulites as shown in Fig. 6, in concurrence with fragmentation of the crystalline lamellae. The role of stress triaxiality is quite obvious in this situation which provides better balance between the normal and tangential stress components as compared with the equatorial situation of Fig. 4. The stress component normal to the crystalline lamellae works as a craze-generating factor as it can be observed in the locus (1) of Fig. 6: crazing clearly occurs at the boundary between two lamella stacks of different stacking directions. Besides, the amplitude images of Fig. 6 reveal a gradual enlargement with increasing strain of the craze between its edge lamellae together with craze propagation along the edge lamellae. In contrast, within regular stacks where craze nucleation is less easy due to suspected better molecular cohesion between neighbor lamellae, the stress component parallel to the lamella surface is promoter of multiple-fracture of the lamellae into fragments as pointed in locus (2) of Fig. 6. Fracture occurs roughly normal to the lamella surface, *i.e.* parallel to the chain stems which are held together in the crystal by weak van der Waals interactions.

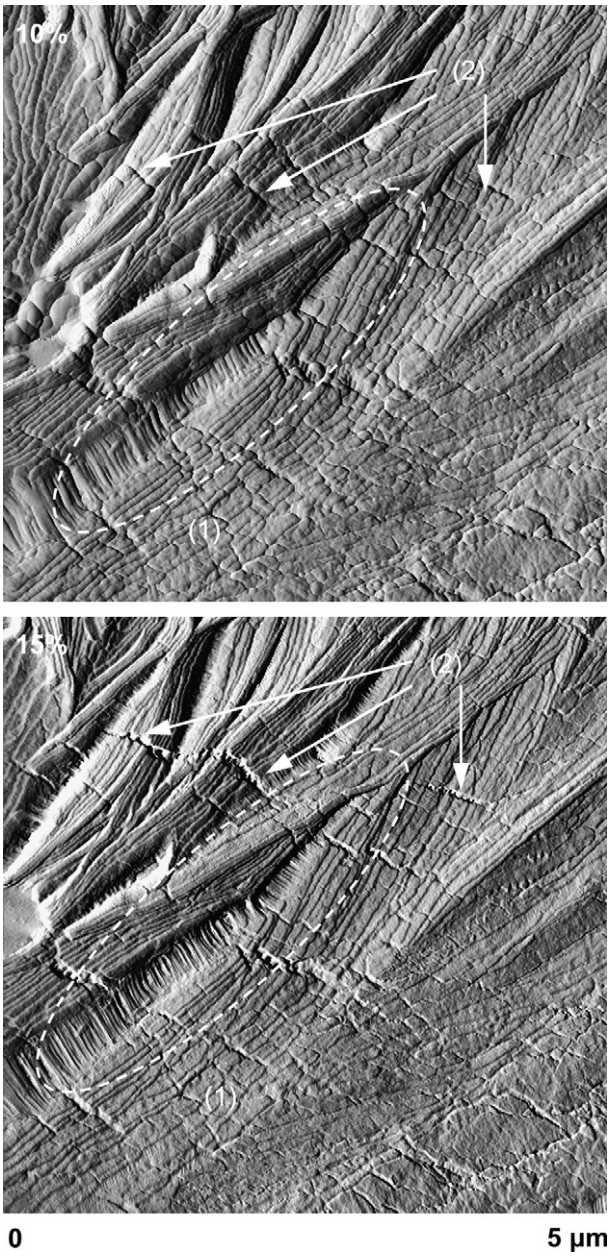

Fig. 6. AFM amplitude images from the diagonal region of a spherulite for strains $\varepsilon = 10$ and 15%: (1) craze nucleated at the boundary of stacks with different lamella orientation; (2) lamella fragmentation within a lamella stack.

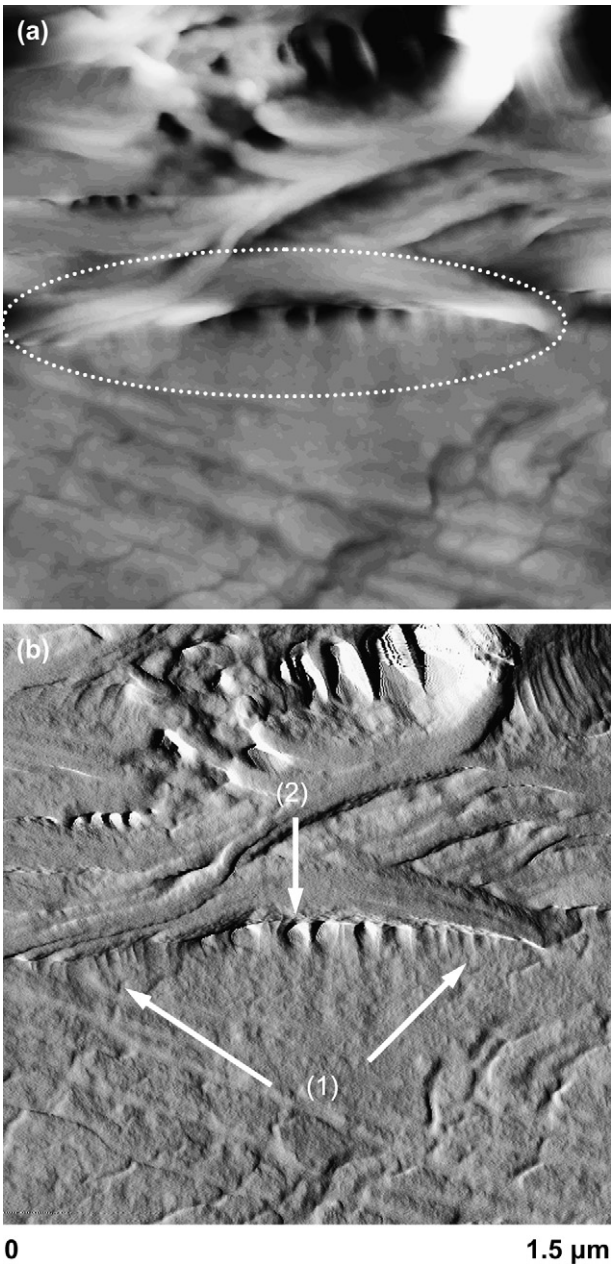

Fig. 7. AFM (a) height and (b) amplitude images from the same zone of equatorial region showing two incipient crazes for a strain $\varepsilon = 15\%$ (Z-range = 1500 nm for the height image).

Examination of Figs. 5 and 6 suggests that crazes arise at the boundary of neighbor stacks having different orientation or at the locus of stacking defects. This is better illustrated in Fig. 7 which reports the height and amplitude images from the equatorial zone containing two nascent crazes. The central craze clearly occurred between two lamella stacks, respectively, edge on, regarding the upper edge, and almost flat on, for the lower edge. The amplitude image of Fig. 7 is particularly worth for understanding the mechanism of initiation of the craze. Indeed, close examination of the tips of the central craze at locus (1) of Fig. 7 reveals nascent microfibrils feeding from the extremities of the crystalline lamellae at the upper edge of the craze. Besides, the microfibrils in the craze core at locus (2) of Fig. 7 display a typical meniscus shape, noticeable on the lower edge of the craze, which is a characteristic feature of craze fibrils [28]. This situation is much likely to result from stress-induced cavitation in an interlamellar amorphous layer.

In the images of Fig. 8, it can be seen how growing crazes in the same lamella stack can join into a single one. Feeding on the same crystalline lamella or set of lamellae ends up in complete transformation of the latter into microfibrils and coalescence of the two growing crazes. Fig. 8 also clearly shows defects in the regular lamellar stacking that may be privileged sites for craze nucleation, as suggested above.

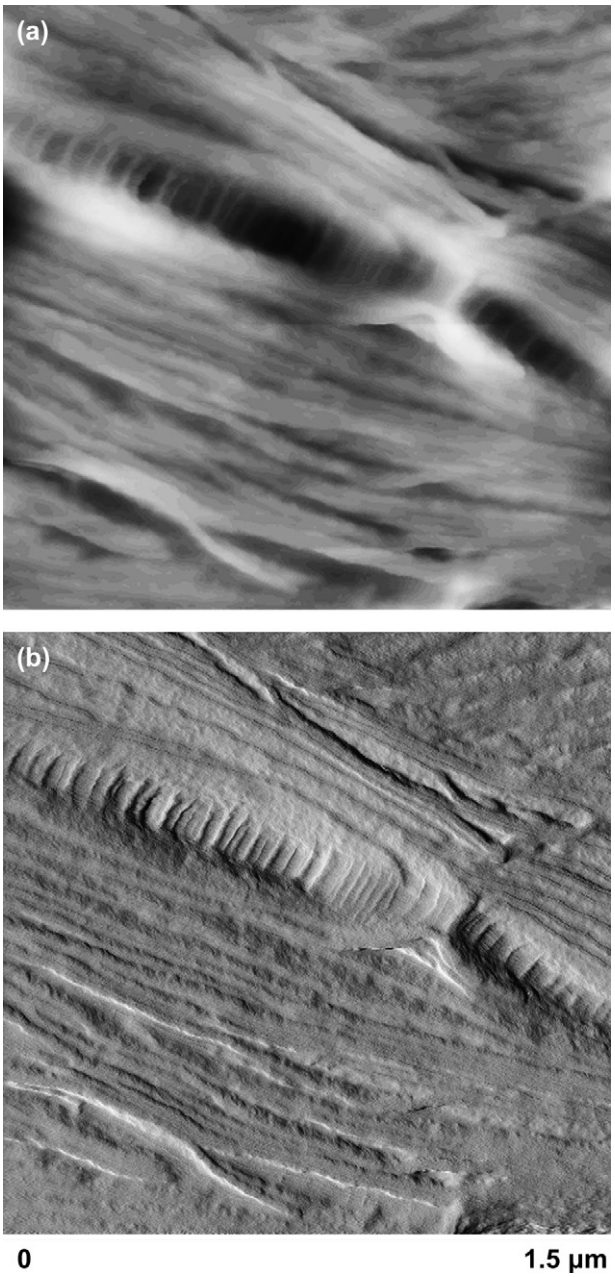

Fig. 8. Small scale AFM (a) height and (b) amplitude images of the same zone showing two crazes in course of coalescence for a strain $\varepsilon = 15\%$ (Z-range = 950 nm for the height image).

4. Concluding discussion

Since the pioneer works by Hild et al. [24] and McLean and Sauer [29], little has been reported on the AFM investigation of the plastic deformation processes in semi-crystalline polymers. The present *in situ* AFM study enabled capturing the following major features of craze development in poly(1-butene) which support the commonly admitted model of crazing of flexible-chain semi-crystalline polymers:

- Crazes formerly arise in the equatorial regions of the spherulites where cavitation can readily occur in the interlamellar amorphous phase thanks to the maximum normal stress acting on the crystalline lamellae. Crazing is much likely initiated between neighbor stacks having different orientations. This may result from a deficiency in molecular connection between the adjacent crystalline lamellae from the two neighbor stacks, as compared with lamellae inside the stacks. Crazes may also occur within lamella stacks, noticeably if lamellae are edge on: in this instance, local stacking irregularities, structural defects within the lamellae or topological weakness in the amorphous layers, such as entanglement density fluctuations, may promote craze initiation.
- The triaxial local stress field generated about the stiff crystalline lamellae is responsible for the opening of crazes in oblique direction with respect to the principal tensile stress due to the normal stress component, concomitantly to lamella fracture resulting from the tangential stress component.
- The characteristic meniscus-like shape of the microfibrils in nascent crazes [28] is thoroughly consistent with the so-called meniscus instability theory of craze formation in glassy polymers.
- Coalescence of crazes can occur owing to a rather high density of craze nucleation. This situation appeared to be favored for crazes growing within the same lamellar stack.

The following points deserve specific comments. The frequently reported observation of very long crazes by transmission electron microscopy (TEM) on ultra-thin films [1,2,13], namely 100–500 nm thick, was not the case in the 100 µm thick PB films of the present AFM study. One may reasonably suspect that both the plane stress conditions and the development of crazes crossing the entire thickness of ultra-thin films under TEM observation promote craze growth at the expense of new craze initiation. Indeed, in the TEM configuration, the area of the craze tip that resists to craze growth is much more restricted than in the case of 3-dimensional lenticular crazes in the bulk. In contrast, TEM observations of microtomic slices from epoxy-embedded bulk deformed materials reveal typical micrometric crazes in the case of polypropylene and high density polyethylene as well [1,30]. The material deformation in the present AFM study seems to takes place under stress conditions close to the bulk triaxial conditions, in spite of the free sample surface from which AFM images are captured. The reason lies in the thickness of the investigated films that is significantly larger than the characteristic craze size. This opportunity for reproducing bulk sample deformation and exploring the incidence of stress triaxiality on the local plastic processes is a major advantage of *in situ* AFM, at the present time.

Craze multiplication seems to be largely dominant over both the coalescence of several crazes into larger ones and the enlargement of individual crazes. It is likely that, only when the craze density reaches a critical value, craze coalescence can turn frequent enough to build up a percolation path leading to the macroscopic rupture of the sample.

Scanning Electron Microscopy (SEM) also proved to be a powerful tool for studying crazing of semi-crystalline polymers [8,12]. The main advantages of AFM over SEM are yet

higher resolution and no sample preparation prior to observation.

The question of the molar mass between entanglements, M_e, is a major one regarding craze initiation and growth. Low M_e values strongly reduce microfibril drawability and thus improve craze stability in glassy polymers. No data are available concerning the PB M_e value, but there is no reason to believe it is much different from that of polypropylene: indeed, both flexible-chain polymers have much similar unperturbed chain dimensions and melt density as well as [31], so that chain coil overlapping and therefore chain entanglement density should be very close. This could be the reason why the PB crazes observed in the present AFM study are not much different from those observed in PP by TEM. Notwithstanding, Plummer and Kausch [18] have pointed out that crystallization conditions may modify the M_e value owing to chain disentanglement from the melt, and this may seriously affect the crazing behavior.

For the sake of comparison, various crystallization treatments have been applied to the PB material with the aim of elaborating samples with smaller spherulite size, namely 25 and 10 μm in average diameter, and consisting of crystalline lamellae of slightly smaller thickness and lower overall crystallinity. Both types of samples displayed much more homogeneous deformation than those of the present study having an average diameter 100–200 μm, without any signs of crazing as already reported for nylon 6 [20]. This striking dependence on spherulite size of the PB plastic behavior seems to be much different from that of β PP which displays a high propensity for crazing irrespective of spherulite size in the range 20–200 μm [8,11,17]. The analysis of these recent experimental findings on PB will be reported in a forthcoming publication [32].

Acknowledgments

The authors are indebted to the European FEDER Program for financial support to the Digital AFM equipment. The Centre National de la Recherche Scientifique and the Région Nord/Pas-de-Calais are also deeply acknowledged for the grant of a doctoral fellowship to C. Thomas. The wise technical assistance of B. Hue and C. Vanmansart from the LSPES laboratory is greatly appreciated for the development of the *in situ* AFM drawing stage. Deep thanks are addressed to Dr. B. Monasse from the Centre de Mise en Forme des Matériaux at Ecole des Mines de Paris (Sophia Antipolis, France) for kindly supplying the PB material.

References

[1] Friedrich K. Adv Polym Sci 1983;52–53:225–74.
[2] Kausch H-H. Polymer fracture. Berlin: Springer Verlag; 1987.
[3] Gloaguen JM, Lefebvre JM. Polymer 2001;42:5841–7.
[4] Muratoglu OK, Argon AS, Cohen RE. Polymer 1995;36:921–30.
[5] Wilbrink MWL, Argon AS, Cohen RE, Weinberg M. Polymer 2001;42:10155–80.
[6] van der Wal A, Nijhof R, Gaymans RJ. Polymer 1999;40:6031–44.
[7] Zuiderduin WCJ, Westzaan C, Huetink J, Gaymans RJ. Polymer 2003;44:261–75.
[8] Aboulfaraj M, G'Sell C, Ulrich B, Dahoun A. Polymer 1995;36:731–42.
[9] Tjong SC, Shen SJ, Li RKY. Polymer 1996;37:2309–16.
[10] Karger-Kocsis J, Varga J. J Appl Polym Sci 1996;62:291–300.
[11] Voitot T. Ph.D. thesis, Reg. no. 2783, Université de Lille, France; 2000.
[12] Henning S, Michler GH. In: Michler GH, Balta-Calleja F-J, editors. Mechanical properties of polymers based on nanostructure and morphology. Boca Raton, FL (USA): CRC Press–Taylor & Francis Group; 2005 [chapter 7].
[13] Plummer CJG, Kausch H-H. Macromol Chem Phys 1996;197:2047–63.
[14] Grein C. Adv Polym Sci 2005;188:43–104.
[15] Labour T, Gauthier C, Séguéla R, Vigier G, Bomal Y. Polymer 2001;42:7127–35.
[16] Karger-Kocsis J. Polym Bull 1996;36:119–24.
[17] Labour T, Séguéla R, Gauthier C, Vigier G, Orange G. J Polym Sci Polym Phys 2002;40:31–42.
[18] Plummer CJG, Kausch H-H. J Macromol Sci Phys 1996;B35:637–57.
[19] Ferreiro V, Pennec Y, Seguela R, Coulon G. Polymer 2000;41:1561–9.
[20] Ferreiro V, Coulon G. J Polym Sci Polym Phys 2004;42:687–701.
[21] Weynant E, Haudin J-M, G'Sell C. J Mater Sci 1980;15:2677–92.
[22] Kaszonyiova M, Rybnikar F, Geil PH. J Macromol Sci Phys 2005;B43:1095–114.
[23] Rubin ID. J Polym Sci Polym Lett 1964;2:747.
[24] Hild S, Gutmannsbauer W, Lüthi R, Fuhrmann J, Güntherodt H-J. J Polym Sci Polym Phys 1996;34:1953–9.
[25] Michler GH, Godehardt R. Cryst Res Technol 2000;35:863–75.
[26] Oderkerk J, de Schaetzen G, Goderis B, Hellemans L, Groeninckx G. Macromolecules 2002;35:6623–9.
[27] Bamberg E, Grippo CP, Wanakamol P, Slocum AH, Boyce MC, Thomas EL. Precis Eng 2006;30:71–84.
[28] Kramer AJ. Adv Polym Sci 1983;52/53:1–56.
[29] McLean RS, Sauer BB. J Polym Sci Polym Phys 1999;37:859–66.
[30] Plummer CJG. Adv Polym Sci 2004;169:75–119.
[31] Brandrup J, Immergut EH. Polymer handbook. 2nd ed. Wiley Interscience; 1975.
[32] Thomas C, Ferreiro V, Coulon G, Seguela R, in preparation.